Engineered antifouling microtopographies: the role of Reynolds number in a model that predicts attachment of zoospores of Ulva and cells of Cobetia marina

Chelsea M. Magin , Christopher J. Long , Scott P. Cooper , Linnea K. Ista , Gabriel P. López & Anthony B. Brennan

Full Terms & Conditions of access and use can be found at
http://www.tandfonline.com/action/journalInformation?journalCode=gbif20

Taylor & Francis
Taylor & Francis Group

Engineered antifouling microtopographies: the role of Reynolds number in a model that predicts attachment of zoospores of *Ulva* and cells of *Cobetia marina*

Chelsea M. Magin[a], Christopher J. Long[b], Scott P. Cooper[b], Linnea K. Ista[c,d], Gabriel P. López[e,f] and Anthony B. Brennan[a,b]*

[a]*J. Crayton Pruitt Family, Department of Biomedical Engineering, University of Florida, Gainesville, Florida, USA;* [b]*Department of Materials Science and Engineering, University of Florida, Gainesville, Florida, USA;* [c]*Center for Biomedical Engineering, The University of New Mexico, Albuquerque, New Mexico, USA;* [d]*Department of Biology, The University of New Mexico, Albuquerque, New Mexico, USA;* [e]*Department of Biomedical Engineering, Duke University, Durham, North Carolina, USA;* [f]*Department of Mechanical Engineering and Materials Science, Duke University, Durham, North Carolina, USA*

A correlation between the attachment density of cells from two phylogenetic groups (prokaryotic Bacteria and eukaryotic Plantae), with surface roughness is reported for the first time. The results represent a paradigm shift in the understanding of cell attachment, which is a critical step in the biofouling process. The model predicts that the attachment densities of zoospores of the green alga, *Ulva*, and cells of the marine bacterium, *Cobetia marina*, scale inversely with surface roughness. The size and motility of the bacterial cells and algal spores were incorporated into the attachment model by multiplying the engineered roughness index (ERI_{II}), which is a representation of surface energy, by the Reynolds number (Re) of the cells. The results showed a negative linear correlation of normalized, transformed attachment density for both organisms with $ERI_{II} \cdot Re$ ($R^2 = 0.77$). These studies demonstrate for the first time that organisms respond in a uniform manner to a model, which incorporates surface energy and the Reynolds number of the organism.

Keywords: biofouling; surface topography; marine bacteria; *Ulva*; *Cobetia marina*; ERI

Introduction

Biofouling, the undesired accumulation of organic molecules and living organisms on a surface (Costerton et al. 1995; Shea et al. 1995; O'Toole et al. 2000), is a significant environmental and economic concern. Biofouling increases drag on vessels by increasing hull roughness, which leads to higher fuel consumption and cost (Townsin 2003; Schultz 2007). The US Naval Sea Systems Command estimates that fuel costs increase 6 to 45% if the hull is fouled, depending on the size of the vessel. Slime layers composed of bacteria and diatoms that develop in the early stages of biofouling (Molino et al. 2009a,b) have been shown to significantly increase hydrodynamic drag and increase fuel consumption (Schultz 2007). Increased fossil fuel consumption is not the only environmental concern raised by biofouling. Hull fouling has been shown to be a primary cause for the introduction and spread of non-indigenous marine species (Otani et al. 2007; Pettengill et al. 2007; Piola and Johnston 2008; Piola et al. 2009; Yamaguchi et al. 2009). The ideal solution to the detrimental effects of biofouling will be a green technology possessing both antifouling (AF)

and fouling-release properties (Genzer and Efimenko 2006; Marmur 2006) to reduce drag and fuel consumption while remaining non-toxic.

Polydimethylsiloxane elastomers (PDMSe), more commonly known as silicones, are currently marketed as non-biocidal marine coatings. These coatings are known to have fouling-release properties (Chaudhury et al. 2005; Holm et al. 2006; Wendt et al. 2006) due to their low surface energy and low modulus (Brady and Singer 2000; Chaudhury et al. 2005); however, they are not inherently AF (Molino et al. 2009a,b). Non-toxic AF technologies that focus on the manipulation of the surface topography of PDMSe have been designed to deter attachment of fouling organisms (Carman et al. 2006; Schumacher et al. 2007a,b, 2008; Long et al. 2010). Carman et al. (2006) presented a biomimetically inspired surface topography, Sharklet AF™, that reduced attachment zoospores of *Ulva* by 86%. *Ulva* is a green alga commonly found in marine biofilms on ships, submarines and other underwater structures. The mature plant of *Ulva* produces motile spores that disperse and colonize surrounding surfaces (Callow and Callow 2000). Evidence suggests that the

---

*Corresponding author. Email: abrennan@mse.ufl.edu
Published online 10 August 2010

swimming spores are able to select a surface suitable for attachment based on topographical, biological (Joint et al. 2002), chemical, and physicochemical cues (Ederth et al. 2008, 2009; Schilp et al. 2009). An empirical relationship called the engineered roughness index (ERI) has been proposed to quantify topographical "roughness" based on parameters that describe surface energy. The results demonstrate a correlation between the attachment behavior of zoospores of *Ulva* and the ERI (Schumacher et al. 2007b). A predictive attachment model was developed based on the second-generation ERI (ERI_{II}) and correctly predicted spore density on three newly designed surface topographies. Four separate sets of *Ulva* attachment data showed excellent correlation ($R^2 = 0.88$) with the attachment model (Long et al. 2010).

The ERI is a dimensionless ratio based on Wenzel's roughness factor (r), the depressed surface area fraction ($1-\Phi_s$), and originally the degrees of freedom of the pattern (df) (Schumacher et al. 2007). Recently, the ERI was extended to include additional topographical designs (Long et al. 2010). The df term was replaced with n, which is the number of unique features in each topography. The ridges topography is comprised of one distinct feature thus an n-value of one. The triangle/pillars topography is composed of two unique features: an equilateral triangle and a round pillar ($n = 2$). ERI_{II} is represented as:

$$ERI_{II} = (r * n)/(1 - \Phi s) \qquad (1)$$

Wenzel's roughness factor (r) is the ratio of the actual surface area to the projected planar surface area (Wenzel 1936). The actual surface area includes the surface area of the feature tops, sides, and depressed surface area between features. The depressed surface fraction ($1-\Phi_s$) described by Bico et al. (1999, 2002), Quére (2008) and others is the ratio of the depressed surface area between features and the projected planar surface area. The depressed surface fraction is equivalent to $1-f_1$, where f_1 is the solid–liquid interface term of the Cassie–Baxter equation for wetting (Cassie and Baxter 1944). The topographies studied were selected to cover a range of ERI_{II} values (Figure 1).

In this study it was hypothesized that the engineered microtopographies in PDMSe would inhibit attachment of marine bacteria and this inhibition would scale with the ERI_{II} value. The marine bacterium *Cobetia marina*, originally isolated from a marine biofilm (Baumann et al. 1983), was used as a model marine fouling organism. The attachment of *C. marina* to defined solid surfaces has been studied extensively through the use of self-assembled mono-layers (SAMs) (Ista et al. 1996, 1999, 2004, 2010) and
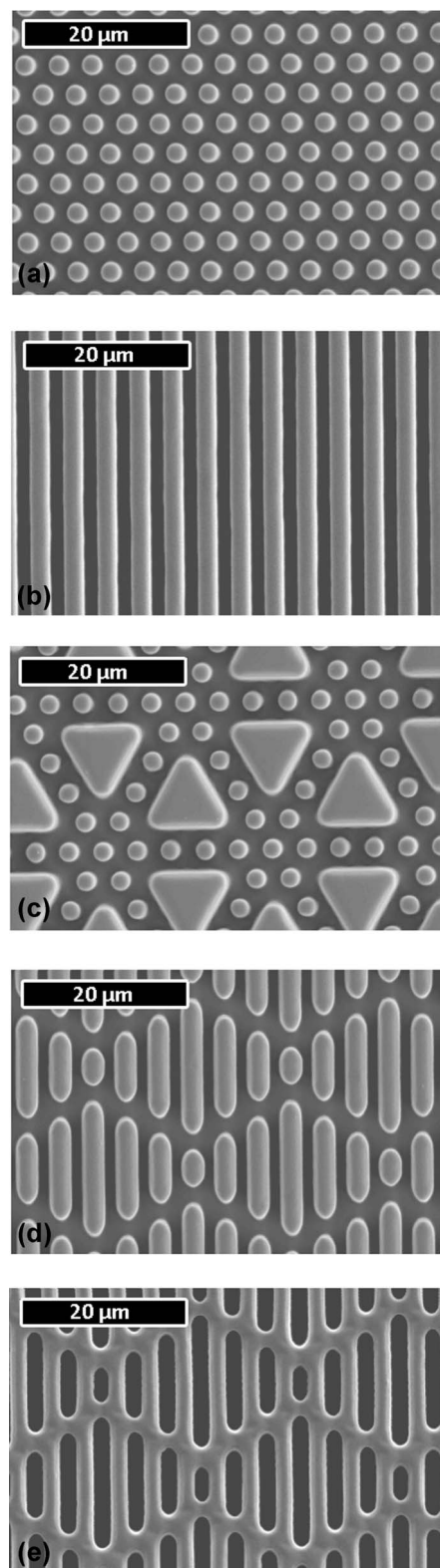

Figure 1.   Scanning electron micrographs of (a) pillars, (b) ridges, (c) triangle/pillars, (d) Sharklet AF™, (e) Recessed Sharklet AF™ surfaces in PDMSe. The topographies of the Sharklet AF™ and the ridges were positioned so that the features were parallel to the direction of flow when mounted in the flow cell.

has been reported to influence secondary colonization (Shea et al. 1995). The present report shows the correlation between the ERI_{II} value and attachment of *C. marina*. Additionally, a single equation is presented that relates attachment densities of spores of *Ulva* and cells of *C. marina* to the ERI_{II} multiplied by the estimated Reynolds number for the individual organisms.

Materials and methods

Materials

The base material used for engineered topographical modification was a platinum-catalyzed PDMSe (Silastic® T-2; Dow Corning Corporation). The elastomer was prepared by hand mixing 10 parts resin and 1 part curing agent by weight for 5 min. The mixture was degassed under vacuum (28–30 in Hg) for 30 min, removed from the vacuum chamber, and poured into negative topographical molds to cure for 24 h at ~22°C.

Pattern designs

The patterns studied included Sharklet AF[TM], recessed Sharklet AF[TM], ridges, pillars, and triangle/pillars (Schumacher et al. 2007b). Sharklet AF[TM] previously described (Carman et al. 2006, Schumacher et al. 2007b) consists of 2 μm wide ribs of various lengths (4, 8, 12, and 16 μm) that are combined by feature length in the following order: 4, 8, 12, 16, 12, 8, and 4 μm at a feature spacing of 2 μm to form a diamond. This diamond of protruding features was the repeat unit for the arrayed pattern. The spacing between each diamond unit was 2 μm. This pattern was inspired by and is similar to the skin of a shark (Bechert et al. 2000) in terms of feature arrangement. Recessed Sharklet AF[TM] is the negative of Sharklet AF[TM]. It has the same arrangement of features indented into the surface instead of protruding out from the surface. Ridges and pillars were designed with an analogous feature spacing of 2 μm. Ridges were continuous in length and separated by 2 μm. The pillars were hexagonally packed so the distance between any two adjacent pillars was 2 μm. The triangle/pillars pattern is a multi-feature pattern formed by replacing a set of six hexagonally packed 2 μm pillars with a 10 μm equilateral triangle. This triangle placement maintained a 2 μm feature spacing between the edges of the triangle and the pillars.

Pattern fabrication

Pattern designs were transferred to photoresist-coated silicon wafers using standard photolithographic techniques described previously (Schumacher et al. 2008). The patterned wafers were deep reactive ion etched using the Bosch process to a depth of approximately 3 μm to create negative molds of the engineered topographies. Wafers were subsequently stripped of photoresist with an O_2 plasma etch. Hexamethyldisilazane was vapor deposited onto the processed wafers to methylate the surfaces and prevent adhesion of PDMSe during the replication process.

Topographical replication

Engineered topographies were transferred to PDMSe by replication of the patterned and etched silicon wafer. The resulting engineered topographies contained features that protrude from or are indented into the surface at a height of approximately 3 μm. Pattern fidelity and feature height were evaluated with light and scanning electron microscopy.

Sample preparation

Samples were provided as smooth PDMSe surrounding two 13 mm × 13 mm squares of engineered topographies of interest adhered to glass coverslips (60 mm × 24 mm, No. 2 thickness). Engineered topographies were attached to glass coverslips using a two-step process previously described (Carman et al. 2006). Topographies (smooth, Sharklet AF[TM], recessed Sharklet AF[TM], ridges, pillars, and triangles/pillars) were randomly assigned to one of two positions on each coverslip. The topographies of Sharklet AF[TM] and ridges were positioned on coverslips so that features were parallel to the direction of flow when mounted in the flow cell. The resulting coverslip was approximately 0.8 mm thick and contained an adhered PDMSe film with two 13 mm × 13 mm square areas containing topography bordered on all sides by smooth (no topography) areas.

Bacteria

Chemostat culture

A logarithmic chemostat culture of *C. marina* ATCC 25374 (American Type Culture Collection, Manassas, VA) strain (Baumann et al. 1983; Arahal et al. 2002) was established in modified basal medium (200 mM NaCl, 50 mM $MgSO_4 \cdot 7H_2O$, 10 mM KCl, 10 mM $CaCl_2 \cdot 2H_2O$, 19 mM NH_4Cl, 0.33 mM K_2HPO_4, 0.1 mM $FeSO_4 \cdot 7H_2O$, 5 mM Tris-HCl (pH 7.5), and 2 mM glycerol) as described previously (Ista et al. 1996). The chemostat was maintained at a flow rate of 1 ml min^{-1} with constant stirring resulting in a cellular concentration of 5×10^7 cells ml^{-1}.

Stationary phase culture

A stationary phase culture of *C. marina* was grown in 1 l of the modified basal medium described above. The inoculated culture grew for 21 h at 25°C while shaking at 400 RPM.

C. marina *attachment assay*

Two bacterial attachment assays were performed with *C. marina*, one using the chemostat culture and one using the stationary phase culture described above. Samples were sterilized by immersion in ethanol for 20 min, soaked in artificial seawater for 1 h and then placed into a laminar flow cell apparatus (Ista et al. 1996) that was mounted on the stage of an optical microscope (Zeiss Axioscope 40). The sample coverslip forms the top plate of the flow chamber to minimize gravitational effects on attachment. The flow cell was then connected to the culture vessel through tubing and a peristaltic pump (Ista et al. 1996, 2004). The cells were introduced into the flow cell at a rate of 2×10^{-5} l s^{-1} for 2 h. Under these conditions for a flat surface, the Reynolds number was $\sim 2 \times 10^{-3}$, indicating laminar flow and the surface shear rate was 6.6×10^{2} s^{-1} (Ista et al. 2004). Bacterial attachment was monitored through a camera attached to a phase contrast microscope. Ten random images were taken of each topography at 15 min intervals. Images were acquired with Axiovision software and processed with ImageJ software (Rasband 1997–2009). Each image was first converted to 8 bit format and then processed using the Fast Fourier Transform (FFT) bandpass filter associated with ImageJ to eliminate background unevenness. The cell densities were determined through direct counting using the ImageJ cell counter plug-in. The attached cells in 10 randomly selected fields of view were counted at each time point. The average number of cells per square millimeter (cells mm^{-2}) was calculated for each replicate. Three replicates were analyzed for each topography. The position of each topography was varied in the flow stream.

Statistical methods

Cell counts are reported as the mean number of cells mm^{-2} from 10 counts on each of three replicate topographies ($n = 30$) with 95% confidence intervals. The cell count data were transformed using a natural logarithm. Statistical differences between surfaces were evaluated with the transformed data using one-way analysis of variance (ANOVA) and Tukey's test for multiple comparisons.

The transformed mean number of cells mm^{-2} for each engineered topography was plotted *vs* time for kinetic analysis. The transformed data were also plotted against the calculated ERI$_{II}$ to determine if any correlations existed between attachment of cells of *C. marina* and the ERI$_{II}$. Regression analysis was performed to evaluate the strength of the correlation.

Results and discussion

Only slight variations in attachment densities were measured over the entire assay period. This includes samples exposed to both logarithmic growth phase and stationary growth phase of *C. marina* (Figure 2). Cells of *C. marina* were calculated to attach at a mean density of 683 ± 79 cells mm^{-2} and 413 ± 51 cells mm^{-2} on the smooth PDMSe at the 120 min time point for the logarithmic growth phase and stationary growth phase, respectively. The cell density for both growth phases was reduced significantly (Figure 3) on all topographies relative to the smooth surface at 120 min. The logarithmic growth phase cell density mm^{-2} was lower on the triangle/pillars (1.7 ± 2.6), Sharklet AF^{TM} (0.1 ± 0.2), and recessed Sharklet AF^{TM} (1.0 ± 1.2) topographies compared to the cell density on pillars (14.2 ± 10.2) and ridges (15.8 ± 7). The attachment density of *C. marina* cells in the stationary growth phase followed the same order, ie, a lower attachment density was measured on triangle/pillars (55 ± 0.3) and Sharklet AF^{TM} (36 ± 0.2) patterns than on pillars (126 ± 0.3) and ridges (166 ± 0.1).

Nearly all of the attached cells were single or in small clusters. Cells appeared to attach in clusters around pillars on the pillar pattern. The majority of cells were attached within the ~ 2 μm wide channels of the ridge patterns. Nearly all cells settled next to the edges of the triangle or clustered around the pillars of the triangle/pillar patterns. Cells did not attach to the tops of the 10 μm triangles. Cells were attached either between the features of the Sharklet AF^{TM} pattern or around the edges of the diamond repeat units. On the recessed Sharklet AF^{TM} pattern cells attached within the ~ 2 μm wide depressions.

The feature dimensions of the topographies used in each study were measured and the average heights, widths and spacings were used to calculate the ERI$_{II}$ value. Due to slight variations in feature height, the value of the ERI$_{II}$ for each pattern varied between the two bacterial attachment assays (Supplementary Tables 1 and 2) [Supplementary material is available *via* a multimedia link on the online article webpage]. Recessed Sharklet AF^{TM} is a newly designed topography with a higher ERI$_{II}$ value (24) than Sharklet AF^{TM} that was included in the logarithmic growth phase attachment assay to further the ERI$_{II}$ series.
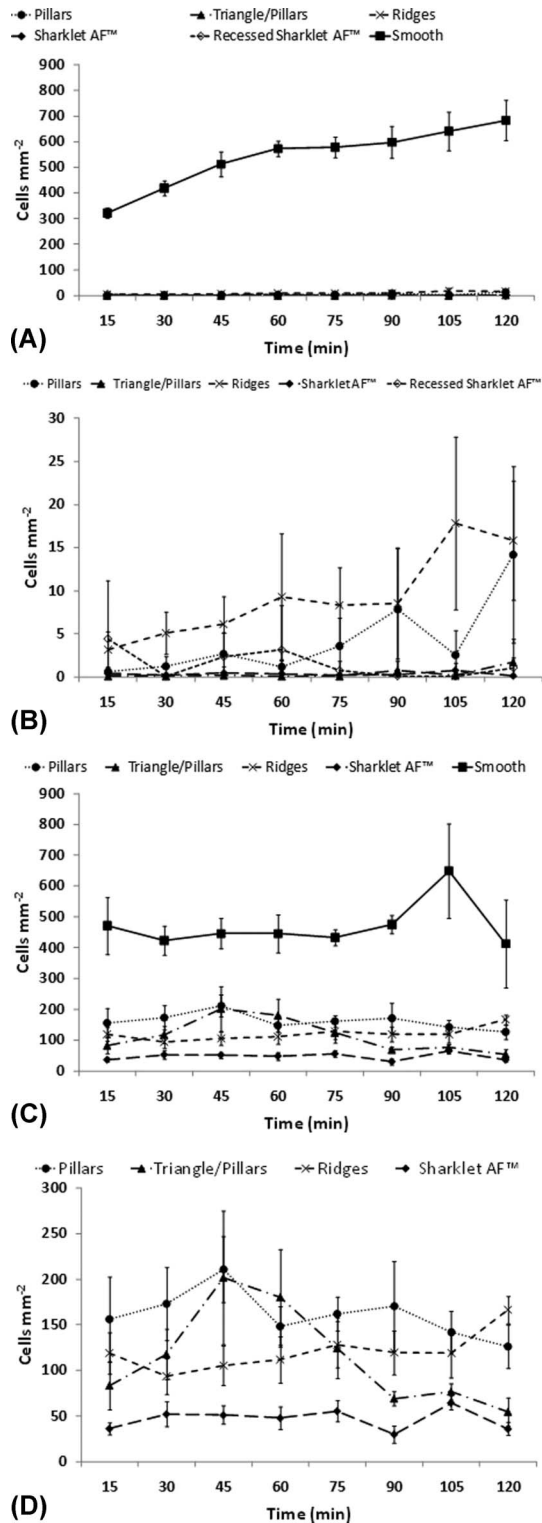
(A)

(B)

(C)

(D)

Figure 2. *C. marina* attachment *vs* time for (A) chemostat culture (logarithmic growth phase), all surfaces; (B) chemostat culture (logarithmic growth phase), topographically modified surfaces only; (C) overnight culture (stationary growth phase), all surfaces; and (D) overnight culture (stationary growth phase), topographically modified surfaces only. Error bars represent 95% confidence intervals.

The natural logarithm of the normalized mean cell density measured on each surface at 120 min was plotted against ERI_{II} of each pattern (Figure 4). A linear regression model was fitted to each set of data. An inverse linear relationship existed between mean cell density and ERI_{II} for bacterial attachment in both the stationary ($R^2 = 0.84$, $p = 0.047$) and logarithmic ($R^2 = 0.40$, $p = 0.038$) growth phases.

The lowest mean cell densities for the logarithmic growth phase of *C. marina* correlated with the highest ERI_{II} values, eg triangle/pillars (5.8), Sharklet AF™ (19), and Recessed Sharklet AF™ (24), but were not different statistically. The second lowest cell densities were measured on ridges and pillars (ERI_{II} values of 5.5 and 3.2, respectively). Cell densities measured in the stationary phase attachment assay followed a similar trend. Triangle/pillars and Sharklet AF™ with the highest ERI_{II} values (6.1 and 13, respectively) had the lowest cell densities. Ridges and pillars had the
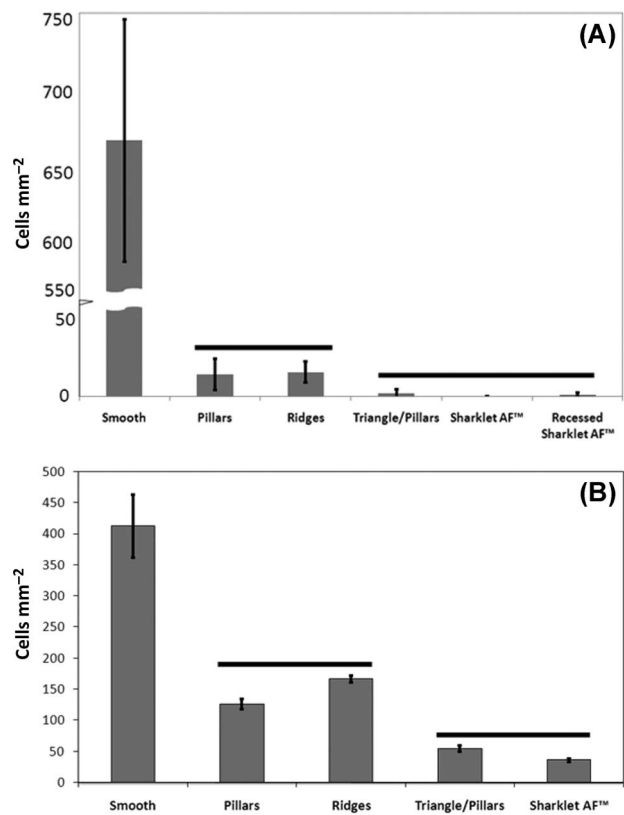

(A)

(B)

Figure 3. *C. marina* attachment data on PDMSe surfaces represented as mean cell density (cells mm^{-2}) $\pm 95\%$ confidence interval ($n = 30$). (A) surfaces exposed to *C. marina* cells in the logarithmic growth phase established in a chemostat culture for 120 min; (B) surfaces exposed to *C. marina* cells in the stationary growth phase established through an overnight culture for 120 min. Solid horizontal bars = statistically different groups (ANOVA $p = 0.05$, Tukey test $p = 0.05$).
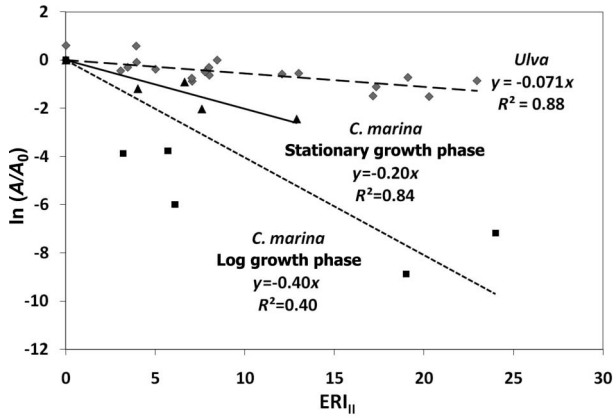
Figure 4. The attachment model shows the correlation between *C. marina* attachment normalized to attachment on a smooth surface and the engineered roughness index (ERI_{II}) at 120 min for the stationary and logarithmic growth phases. Plotted is the calculated ERI_{II} for each pattern tested *vs* the natural logarithm of the experimental mean bacterial cell density at the 120 min time point minus the mean bacterial cell density on a smooth surface at the same time point ($\ln(A/A_0)$) ($n = 30$). Data for attachment of zoospores of *Ulva*, taken from Long et al. (2010) are also plotted.

next highest ERI_{II} values (5.9 and 3.2) and the second lowest attachment densities.

The regression analysis for cell attachment to the surfaces established a statistically significant trend for both the logarithmic growth phase and stationary growth phase. These trends were analyzed in terms of the attachment model as Equations (2) and (3). The variable A is the attachment on a surface with a given ERI_{II} value and A_0 is the attachment on a smooth surface ($ERI_{II} = 0$).

$$\ln\left(\frac{A}{A_0}\right) = -0.40 * ERI_{II} \qquad (2)$$

$$\ln\left(\frac{A}{A_0}\right) = -0.20 * ERI_{II} \qquad (3)$$

Adhesion of marine bacteria to surfaces has been attributed to many factors, viz. the substratum composition (Ista et al. 2004, Ekblad et al. 2008), surface chemistry (Ista et al. 1996, 1999; Poolman et al. 2004; Cordiero et al. 2009), substratum mechanical properties (Ekblad et al. 2008; Cordiero et al. 2009), and surface roughness (Kerr and Cowling 2003). Substratum composition, substratum mechanical properties and surface chemistry were kept constant in this study by using PDMSe for all surfaces. Surface roughness was systematically studied by using the ERI_{II} algorithm to describe engineered microtopographies.

Plots of *C. marina* cell attachment over time indicated that cells in both the logarithmic and stationary growth phase reacted to surface topography nearly instantaneously (Figure 2). Bacterial attachment density did not change significantly from the first time point (15 min) to the last (120 min). This response was due to physical, not chemical, changes in the substratum. These results are consistent with the work of Kerr and Cowling (2003) in which the effect of surface roughness on bacterial adhesion was observed to be almost instantaneous.

Cell densities measured at the last time point indicated that all topographies showed a statistically significant reduction in the density of attached cells in both growth phases relative to the smooth surface (Figure 3). A fairly strong inverse linear relationship existed between the natural logarithm of the mean cell density and ERI_{II} value for both bacterial attachment assays (Figure 4). These relationships, however, did not follow the same regression line. Attachment of cells established in a chemostat culture (logarithmic growth phase) correlated with a line with a steeper slope ($m = -0.40$) than the cells in the stationary growth phase ($m = -0.20$). The slopes of these lines were both different from the slope of the regression line for attachment of spores of *Ulva* vs ERI_{II} value ($m = -0.071$) from four separate studies reported in previous work (Long et al. 2010).

It is possible that the slope of the line in the attachment model (m) encompasses the organism's sensitivity to a surface (Equation 4).

$$\ln\left(\frac{A}{A_0}\right) = -m * ERI_{II} \qquad (4)$$

This sensitivity could be related to a number of factors including the size and shape (Kerr and Cowling 2003; Carman et al. 2006), motility (Shea et al. 1995), and surface chemistry (Shea et al. 1991; Ista et al. 2004; Poolman et al. 2004; Cordiero et al. 2009; Ista et al. 2010) of the attaching organism and/or conditioning of the surface by the culture medium and secreted products (Jain and Bhosle 2009). It has been observed that in late stationary phase, cells of *C. marina* tend to shrink to approximately 1 μm in diameter and take on a more rounded shape. The same cells in the logarithmic growth phase are rod-shaped, approximately 2 μm in length and often joined in pairs. This size and shape difference may influence bacterial attachment. The results from this study also showed stationary phase cells adhered to hydrophobic topographic surfaces in higher numbers than logarithmic-phase cells. The higher densities of bacteria attached to surfaces exposed to the stationary phase culture could

be due to the fact that there were simply more bacteria cells in the overnight culture than the chemostat culture. A standard overnight culture has approximately 10^9 cells ml^{-1} whereas the chemostat is maintained at approximately 10^7 cells ml^{-1}. The influence of size and shape of the organisms moving in a fluid can be described by the Reynolds number.

The Reynolds number is the ratio of inertial forces to viscous forces in fluid flow. Viscous forces dominate inertial forces in conditions such as those experienced by cells of *C. marina* and spores of *Ulva* while moving through water (Purcell 1977; Berg 1983; Dusenbery 2009). Therefore bacteria and spores operate at low Reynolds number. Alternatively, the Reynolds number can be considered to represent the scale separation in the flow. That is to say the bacteria and algal spores are not large compared to the smallest scales in the flow at which viscosity dissipates kinetic energy. The *Ulva* spore is a flagellated cell capable of propelling itself through the water. A recent report proposed that the flagellar motion of the swimming unicellular alga, *Chlamydomonas*, is coupled to its hydrodynamic environment (Polin et al. 2009). The bacterial cells in this study were not flagellated. The Reynolds numbers for the swimming *Ulva* spore and the cells of *C. marina* in both growth phases were calculated using the following equation:

$$Re = \frac{\rho V L}{\mu} \quad (5)$$

where ρ and μ are the density and viscosity of the fluid used in the assay, V is the velocity of the organism relative to that of the fluid, and L is the characteristic length of the organism (see Supplementary Information for full calculation) [Supplementary material is available *via* a multimedia link on the online article webpage]. The characteristic length is a dimension relevant to the geometry of the flow; in this case it is the diameter of the body moving through the fluid. The characteristic length, ie the diameter of the spore body at its widest point, and the velocity of the *Ulva* spore were taken to be 5 μm and 150 μm s^{-1}, respectively (Callow et al. 2002; Heydt et al. 2009). The characteristic length of *C. marina* varies with growth phase. It is 2 μm for the logarithmic growth phase and 1 μm for the stationary growth phase. The velocity of the bacterial cells relative to the fluid near the wall was estimated to be 20% of the average fluid velocity in the flow cell. When the bacterial cells enter the boundary layer near the wall, the velocity will be considerably less than the average bulk velocity due to the no-slip boundary condition. The flow velocity of the fluid, which is a key component of the Reynolds number, has been demonstrated to affect the attachment density of

spores of *Ulva* (Granhag et al. 2007). The size and motion of the organisms were incorporated into the slope of the attachment model by multiplying the $\mathrm{ERI_{II}}$ value by the Reynolds number of the organism.

$$m = m' Re \quad (6)$$

$$\ln\left(\frac{A}{A_0}\right) = -(m' Re) * \mathrm{ERI_{II}} \quad (7)$$

The incorporation of the Reynolds number into the attachment model allowed four separate spore attachment assays (Schumacher et al. 2007, 2008; Long et al. 2010) to be combined with both *C. marina* attachment assays into a single data set that yields a regression with high correlation to $\mathrm{ERI_{II}} \cdot Re$ ($R^2 = 0.77$) (Figure 5).

Further work is planned to investigate the role of the slope of the attachment model line as an indicator of the sensitivity of an organism to a surface. This work could include attachment of different species or organisms such as new or mutant strains of bacteria to elucidate which factors contribute to the sensing of topographically modified surfaces. It could also include altering the flow conditions to change the organism's Reynolds number and investigate the role of the hydrodynamic environment on biological attachment.

Microtopographies created in non-toxic materials such as PDMSe are a green alternative to biocidal methods for reducing biofouling. The attachment model has been demonstrated to correlate the $\mathrm{ERI_{II}}$ value multiplied by the Reynolds number for the organism to the attachment density of cells from two kingdoms (Bacteria and Plantae). An inverse linear
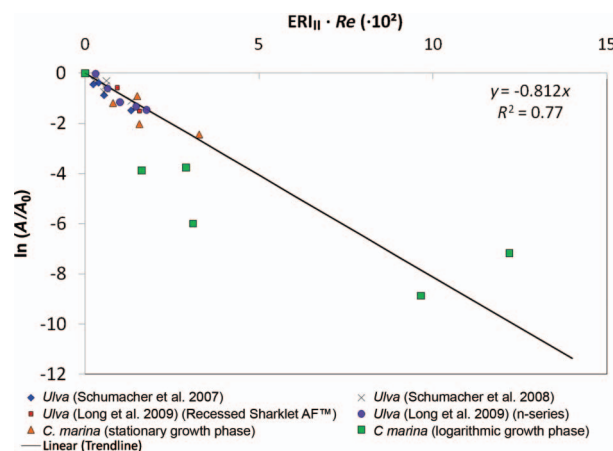

Figure 5. The attachment model shows the correlation between attachment of zoospores of *Ulva* and cells of *C. marina* normalized to attachment on a smooth surface and the engineered roughness index ($\mathrm{ERI_{II}}$) multiplied by the Reynolds number of the organism.

relationship exists between mean cell densities for the two different organisms and $ERI_{II} \cdot Re$. Plots of the attachment of *C. marina* over time indicate that both logarithmic phase and stationary phase cells reacted to surface topography within 15 min of exposure to the surface. At the 120 min time point, all topographically modified surfaces showed a statistically significant reduction in attachment compared to smooth surfaces for both bacterial attachment assays. The incorporation of the Reynolds number into the attachment model created a regression model with a high correlation of attachment for spores of *Ulva* and cells of *C. marina* in both growth phases to $ERI_{II} \cdot Re$.

Acknowledgements

References

Arahal DR, Castillo AM, Ludwig W, Schleifer KH, Ventosa A. 2002. Proposal of *Cobetia marina* gen. nov., comb. nov. within the family Halomonadaceae, to include the species *Halomonas marina*. Syst Appl Microbiol 25: 207–211.

Baumann L, Bowditch RD, Baumann P. 1983. Description of *Deleya* gen. nov. created to accommodate the marine species *Alcaligenes aestus, A. pacificus, A. cupidus, A. venustus*, and *Pseudomonas marina*. Int J Syst Bacteriol 33:793–802.

Bechert DW, Bruse M, Hage W. 2000. Experiments with three-dimensional riblets as an idealized model of shark skin. Exp Fluids 28:403–412.

Berg HC. 1983. Random walks in biology. Princeton, NJ: Princeton University Press.

Bico J, Marzolin C, Quere D. 1999. Pearl drops. Europhys Lett 47:220–226.

Bico J, Thiele U, Quere D. 2002. Wetting of texture surfaces. Colloids Surf A 206:41–46.

Brady RF, Singer IL. 2000. Mechanical factors favoring release from fouling release coatings. Biofouling 15:73–81.

Callow ME, Callow JA. 2000. Substratum location and zoospore behaviour in the fouling alga *Enteromorpha*. Biofouling 15:49–56.

Callow ME, Jennings AR, Brennan AB, Seegert CA, Gibson AL, Wilson LH, Feinberg AW, Baney R, Callow JA. 2002. Microtopographic cues for settlement of zoospores of the green fouling alga *Enteromorpha*. Biofouling 18: 237–245.

Carman ML, Estes TG, Feinberg AW, Schumacher JF, Wilkerson W, Wilson LH, Callow ME, Callow JA, Brennan AB. 2006. Engineered antifouling microtopographies – correlating wettability with cell attachment. Biofouling 22:11–21.

Cassie ABD, Baxter S. 1944. Wettability of porous surfaces. Trans Faraday Soc 40:546–551.

Chaudhury MK, Finaly JA, Chung JY, Callow ME, Callow JA. 2005. The influence of elastic modulus and thickness on the release of the soft-fouling green alga *Ulva linza* (syn. *Enteromorpha linza*) from poly(dimethylsiloxane) (PDMS) model networks. Biofouling 21:41–48.

Cordiero A, Nitschke M, Janke A, Helbig R, D'Souza F, Donnelly G, Willemsen P, Werner C. 2009. Fluorination of poly(dimethylsiloxane) surfaces by low pressure CF4 plasma – physicochemical and antifouling properties. Express Polym Lett 3:70–83.

Costerton JW, Lewandowski Z, Caldwell DE, Korber DR, Lappin-Scott HM. 1995. Microbial biofilms. Annu Rev Microbiol 49:711–745.

Dusenbery DB. 2009. Living at micro scale. The unexpected physics of being small. London, UK: Harvard University Press.

Ederth T, Nygren P, Pettitt ME, Östblom M, Du C-X, Broo K, Callow ME, Callow JA, Liedberg B. 2008. Anomolous settlement behaviour of *Ulva linza* zoospores on cationic oligopeptide surfaces. Biofouling 24: 303–312.

Ederth T, Pettitt ME, Nygren P, Du C-X, Ekblad T, Zhou Y, Falk M, Callow ME, Callow JA, Liedberg B. 2009. Interactions of zoospores of *Ulva linza* with arginine-rich oligopeptide monolayers. Langmuir 25:9375–9383.

Ekblad T, Bergstrom G, Ederth T, Conlan SL, Mutton R, Clare AS, Wang S, Liu Y, Zhao Q, D'Souza F, et al. 2008. Poly(ethylene glycol)-containing hydrogel surfaces for antifouling applications in marine and freshwater environments. Biomacromolecules 9:2775–2783.

Genzer J, Efimenko K. 2006. Recent developments in superhydrophobic surfaces and their relevance to marine fouling: a review. Biofouling 22:339–360.

Granhag LM, Larsson AI, Jonsson PR. 2007. Algal spore settlement and germling removal as a function of flow speed. Mar Ecol Prog Ser 344:63–69.

Heydt M, Divos P, Grunze M, Rosenhahn A. 2009. Analysis of holographic microscopy data to quantitatively investigate three-dimensional settlement dynamics of algal zoospores in the vicinity of surfaces. Eur Phys J E 30: 141–148.

Holm ER, Kavanagh CJ, Meyer AE, Wiebe D, Nedved BT, Wendt D, Smith C, Hadfield MG, Swain G, Wood CD, et al. 2006. Interspecific variation in patterns of adhesion of marine fouling to silicone surfaces. Biofouling 22: 233–243.

Ista LK, Perez-Luna VH, Lopez GP. 1999. Surface-grafted, environmentally sensitive polymers for biofilm release. Appl Environ Microbiol 65:1603–1609.

Ista LK, Mendez S, Lopez GP. 2010. Attachment and detachment of bacteria on surfaces with tunable and switchable wettability. Biofouling 26:111–118.

Ista LK, Fan H, Baca O, Lopez GP. 1996. Attachment of bacteria to model solid surfaces: oligo(ethylene glycol) surfaces inhibit bacterial attachment. FEMS Microbiol Lett 142:59–63.

Ista LK, Callow ME, Finlay JA, Coleman SE, Nolasco AC, Simons RH, Callow JA, Lopez GP. 2004. Effect of substratum surface chemistry and surface energy on attachment of marine bacteria and algal spores. Appl Environ Microbiol 70:4151–4157.

Jain A, Bhosle NB. 2009. Biochemical composition of the marine conditioning film: implications for bacterial adhesion. Biofouling 25:13–19.

Joint I, Tait K, Callow ME, Callow JA, Milton D, Williams P, Camara M. 2002. Cell-to-cell communication across the prokaryote–eukaryote boundary. Science 298:1207.

Kerr A, Cowling MJ. 2003. The effects of surface topography on the accumulation of biofouling. Philos Mag 83:2779–2795.

Long CJ, Schumacher JF, Robinson P, II, Finaly JA, Callow ME, Callow JA, Brennan AB. 2010. A model that predicts the attachment behavior of *Ulva linza* zoospores on surface topography. Biofouling 26:411–419.

Marmur A. 2006. Super-hydrophobicity fundamentals: implications to biofouling prevention. Biofouling 22:107–115.

Molino PJ, Campbell E, Wetherbee R. 2009a. Development of the initial diatom microfouling layer on antifouling and fouling-release surfaces in temperate and tropical Australia. Biofouling 25:685–694.

Molino PJ, Childs S, Hubbard MRE, Carey JM, Burgman MA, Wetherbee R. 2009b. Development of the primary bacterial microfouling layer on antifouling and fouling release coatings in temperate and tropical environments in Eastern Australia. Biofouling 25:149–162.

O'Toole G, Kaplan HB, Kolter R. 2000. Biofilm formation as microbial development. Annu Rev Microbiol 54:49–79.

Otani M, Oumi T, Uwai S, Hanyuda T, Prabowo RE, Yamaguchi T, Kawai H. 2007. Occurrence and diversity of barnacles on international ships visiting Osaka Bay, Japan, and the risk of their introduction. Biofouling 23:277–286.

Pettengill JB, Wendt DE, Schug MD, Hadfield MG. 2007. Biofouling likely serves as a major mode of dispersal for the polychaete tubeworm *Hydroides elegans* as inferred from microsatellite loci. Biofouling 23:161–169.

Piola RR, Johnston EL. 2008. The potential for translocation of marine species via small-scale disruptions to antifouling surfaces. Biofouling 24:145–155.

Piola RF, Dafforn KA, Johnston EL. 2009. The influence of antifouling practices on marine invasions. Biofouling 25:633–644.

Polin M, Tuval I, Drescher K, Gollub J, Goldstein RE. 2009. *Chlamydomonas* swims with two ''gears'' in a eukaryotic version of run-and-tumble locomotion. Science 325:487–490.

Poolman B, Spitzer JJ, Wood JM. 2004. Bacterial osmosensing: roles of membrane structure and electrostatics in lipid-protein and protein-protein interactions. Biochem Biophys Acta 1666:88–104.

Purcell E. 1977. Life at low Reynolds number. Am J Phys 45:3–11.

Quère D. 2008. Wetting and roughness. Annu Rev Mater Res 38:71–99.

Rasband WS. 1997–2009. ImageJ. Bethesda, MD: National Institutes of Health.

Schilp S, Rosenhahn A, Pettitt ME, Bowen J, Callow ME, Callow JA, Grunze M. 2009. Physicochemical properties of (ethylene glycol)-containing self-assembled monolayers relevant for protein and algal cell resistance. Langmuir 25:10077–10082.

Schultz MP. 2007. Effects of coating roughness and biofouling on ship resistance and powering. Biofouling 23:331–341.

Schumacher JF, Long CJ, Callow ME, Finaly JA, Callow JA, Brennan AB. 2008. Engineered nanforce gradients for inhibition of settlement (attachment) of swimming algal spores. Langmuir 24:4931–4937.

Schumacher JF, Aldred N, Callow ME, Finaly JA, Callow JA, Clare AS, Brennan AB. 2007a. Species-specific engineered antifouling topographies: correlations between the settlement of algal zoospores and barnacle cyprids. Biofouling 23:307–317.

Schumacher JF, Carman ML, Estes TG, Feinberg AW, Wilson LH, Callow ME, Callow JA, Finlay JA, Brennan AB. 2007b. Engineered antifouling microtopographies – effect of feature size, geometry, and roughness on settlement of zoospores of the green alga *Ulva*. Biofouling 23:55–62.

Shea C, Lovelace L, Smith-Somerville H. 1995. *Deleya marina* as a model organism for studies of bacterial colonization and biofilm formation. J Ind Microbiol 15:290–296.

Shea C, Nunley J, Williamson J, Smith-Somerville H. 1991. Comparison of the adhesion properties of *Deleya marina* and the exopolysaccharide-defective mutant strain DMR. Appl Environ Microbiol 57:3107–3113.

Townsin RL. 2003. The ship hull fouling penalty. Biofouling 19(Suppl):9–15.

Wendt DE, Kowalke GL, Kim J, Singer IL. 2006. Factors that influence elastomeric coating performance: the effect of coating thickness on basal plate morphology, growth and critical removal stress of the barnacle *Balanus amphitrite*. Biofouling 22:1–9.

Wenzel RN. 1936. Resistance of solid surfaces to wetting by water. Indust Eng Chem 28:988–994.

Yamaguchi T, Prabowo RE, Ohshiro Y, Shimono T, Jones D, Kawai H, Otani M, Oshino A, Inagawa S, Akaya T, Tamura I. 2009. The introduction to Japan of the Titan barnacle, *Megabalanus coccopoma* (Darwin, 1854) (Cirripedia: Balanomorpha) and the role of shipping in its translocation. Biofouling 25:325–333.